JOURNAL OF PROPULSION AND POWER
Vol. 22, No. 3, May–June 2006

Catalytic Combustion of Rich Methane/Oxygen Mixtures for Micropropulsion Applications

Scott J. Volchko,* Chih-Jen Sung,† and Yimin Huang‡
Case Western Reserve University, Cleveland, Ohio 44106
and
Steven J. Schneider§
NASA John H. Glenn Research Center at Lewis Field, Cleveland, Ohio 44135

In an effort to aid the development of micropropulsion devices with a thrust level of 1–10 mN, as required by the next generation of miniaturized satellites and spacecraft, the combustion of rich methane/oxygen propellant mixtures in platinum microtubes with inside diameters of 0.4 and 0.8 mm is characterized. All of the mixtures tested had equivalence ratios beyond the corresponding rich flammability limits. Experimental results show that catalytic reactions could support combustion in mixtures even when gas-phase chemistry does not play a significant role. The effects of varying equivalence ratio, pressure, mass flow rate, and tube diameter on the critical temperature leading to catalytic ignition are systematically investigated. Furthermore, the effects of doping the methane/oxygen mixture with hydrogen are explored, demonstrating a substantial reduction in the ignition temperature with hydrogen addition. Microtube performance in terms of available thrust, specific impulse, and power required for preheating the microtube are also discussed. By the use of a plug flow model, the experimental conditions are simulated with detailed gas-phase/surface chemistry, thermodynamic properties, and transport properties. The computational results generally support the experimental findings.

Introduction

THERE has been increasing interest in developing smaller-scale satellites and spacecraft in recent years.[1] Their propulsion systems will be required to provide very low thrust on the order of a few millinewtons. Microspacecraft likely to be developed will have a total mass range of 10–100 kg, whereas smaller nanospacecraft will have a total mass range of 5–20 kg (Ref. 2). Micropropulsion needs can be broken up into three different types: 1) orbit insertion or transfer, 2) stationkeeping and drag compensation, and 3) attitude control.[3] The main benefits of small-scale propulsion devices are reduced life-cycle costs, potential for mass production, and reduced launch costs.[1] In addition, grouping micropropulsion devices into arrays and controlling individual or groups of thrusters allows for thrust vectoring and acceleration shock control for larger thrust applications.[1] With the desire to develop miniaturized satellites and spacecraft, the challenges of developing the corresponding propulsion and power systems must be realized.

Micropropulsion devices can be divided into two different classes: electrical or nonchemical and chemical thrusters. The current state-of-the-art nonchemical micropropulsion devices include vaporizing liquid thrusters, compact plasma accelerators, laser ablation, ion propulsion, radioisotope electronic propulsion, digital propulsion, micro cold gas, and subliming solid micropropulsion.[2,4–7] Typically electric propulsion devices use electric energy from a stored source to eject propellant mass.[3] Other forms of nonchemical microthrusters were also discussed in Ref. 2. Although the field of micropropulsion is relatively new, microscale chemical propulsion devices that utilize monopropellants,[2,8,9] bipropellants,[2,10–12] solid propellants,[2] and hybrid propellants[13] have already been developed, and more efficient versions are currently being developed. Recent reviews on chemical microthrusters can also be found in Refs. 14–16.

Reducing the scale of conventional combustors will not be a practical means of developing chemical micropropulsion devices. As the combustor size is scaled down, the surface-to-volume ratio increases. Because the heat loss rate scales with the surface area and the heat release rate scales with volume, the heat loss will eventually dominate, thus quenching the flame.[17] The limitations placed on combustion chamber size prevent scaling conventional designs down to microcombustors. To develop a microthruster effectively, a viable alternative to the conventional design must be developed. To overcome the flame quenching effects common in small-scale microcombustors, thermal management[18,19] and operation with near-stoichiometric mixtures and/or highly energetic fuels can be used to enhance gas-phase combustion.[14,15] Another viable combustion alternative is to take advantage of surface catalysis, which is the emphasis of the present study.

It is well known that the use of certain catalyst materials enables the initiation and progress of combustion reactions even when the characteristic combustor dimension is smaller than the quenching distance/diameter and/or the mixture composition is beyond the flammability limit. Catalyzed ignition/combustion using a miniature tube apparatus, which is fabricated from known catalyst materials, is, therefore, proposed.[10,20] Once catalyzed ignition is established in a microtube, the reacting gases can be used for generating thrust in the micropropulsion device, or they can be propagated into the combustion chamber for ignition in larger-thrust class rockets. The latter would benefit all rocket propulsion systems through the elimination of high-voltage discharges for spark ignition. The high current density required for resistive heating of the catalyst results in low current requirements due to the small cross sections of these devices. In addition, the simplicity in microtube geometry facilitates fundamental, detailed simulations to compare with experimental data for validation purposes. The present work focuses on the investigation

Presented as Paper 2005-3924 at the AIAA/ASME/SAE/ASEE 41st Joint Propulsion Conference and Exhibit, Tucson, AZ, 11–13 July 2005; received 31 August 2005; revision received 1 December 2005; accepted for publication 23 December 2005.

*Graduate Student, Department of Mechanical and Aerospace Engineering; sxv29@case.edu.
†Associate Professor, Department of Mechanical and Aerospace Engineering; cjs15@case.edu. Senior Member AIAA.
‡Research Associate, Department of Mechanical and Aerospace Engineering; yxh29@case.edu.
§Aerospace Engineer, On-Board Propulsion Branch; Steven.J.Schneider@grc.nasa.gov. Associate Fellow AIAA.

of achieving ignition and sustained combustion in such a microtube geometry under varying conditions.

In earlier studies,[10,20] fuel-rich H_2/O_2 mixtures in platinum and palladium microtubes were investigated. Fuel-rich conditions were of particular interest to prevent oxidation loss of catalyst material. A portion of the microtube was resistively heated to achieve catalytic ignition. It was found that the critical ignition temperature for a 0.4-mm Pt tube ranged from 410 to 480 K at 0.0136-atm ambient conditions with equivalence ratios between 6.7 and 13.3 and from 310 to 380 K for atmospheric ambient conditions with equivalence ratios between 8 and 20. For a 0.8-mm Pd tube, the critical ignition temperature ranged from 310 to 470 K at ambient pressure of 0.0136 atm with equivalence ratios between 8 and 40 and from 330 to 430 K under ambient pressure of 1.0 atm with equivalence ratios between 8 and 13.3. Microtube performance for the 0.8 mm Pt tube in a vacuum showed that 1–10 mN of thrust could be generated with a maximum specific impulse of 300 s with H_2/O_2 propellants. For the range of mass flow rates tested, the 0.4-mm Pt tube showed a maximum thrust of about 1.1 mN with a maximum specific impulse of 220 s with H_2/O_2 propellants. It was also demonstrated[10,20] that whereas heat flux is needed to bring the mixture to a critical ignition temperature, the power requirements for catalyzed bipropellant microtubes will be much less than that required for electric propulsion devices.

The present investigation seeks to extend previous endeavors by studying fuel-rich CH_4/O_2 mixtures. The decision to use methane is partially driven by the NASA Mars initiative.[21] The current Mars exploration calls for producing methane in situ by reacting CO_2 from the Mars environment with stored or onboard produced H_2 (Ref. 21) via, for example, the so-called Sabatier reaction: $CO_2 + 4H_2 \rightarrow CH_4 + 2H_2O$. The H_2O formed from the reaction of CO_2 and H_2, will then be decomposed to O_2 and H_2, yielding the O_2 required for reaction with the produced CH_4 (Ref. 21). The methane and oxygen generated will be used as propellants to power spacecraft from the surface of Mars into orbit. The objective of this paper is to aid the development of a microthruster for space-based applications capable of generating thrust between 1 and 10 mN with a maximum specific impulse of ~200 s using methane and oxygen propellants.

The results presented in this paper consist of an experimental evaluation of the critical temperature to achieve catalytic ignition for rich CH_4/O_2 mixtures in platinum microtubes with 0.4- and 0.8-mm inside diameters. Catalytic ignition was realized by resistively heating the microtube as premixed gas flowed through the tube. Tube temperature distribution and inlet pressure were monitored for an indication of exothermic reactions. Experiments were performed at ambient pressures of both 1.0 and 0.0136 atm. The ability for initiated reactions to self-sustain without heat input was explored. In addition, the effect of adding a small amount of hydrogen to the rich CH_4/O_2 mixtures was investigated. The available thrust and specific impulse for the vacuum tests (ambient pressure of 0.0136 atm) were assessed. A plug-flow model with detailed gas-phase and surface chemistry, thermodynamic properties, and transport properties was also used to model the experimental work. The following sections include the details of experimental setup and computational methodology, as well as a discussion of the experimental and computational results.

Premixed Flame Characteristics of Rich CH_4/O_2 Mixtures

Studies have shown that as tube size is progressively decreased, premixed flames eventually cannot propagate through tubes.[22,23] The corresponding critical tube diameter below which a flame can no longer propagate is then defined as the quenching diameter. This quenching diameter is caused by excessive heat transfer from the flame front to the walls of the tube, as well as removal of radicals near the wall surface. The effects of wall quenching are important in determining not only the flammability limits but also ignition characteristics.[22,23] It has been shown that the quenching diameter is on the same order as the flame thickness.[22] Because the flame thickness is inversely proportional to the burning rate, it decreases with increasing burning intensity. Therefore, near stoichiometric flames will have relatively smaller flame thicknesses, whereas near-limit flames will have appreciably larger flame thicknesses.

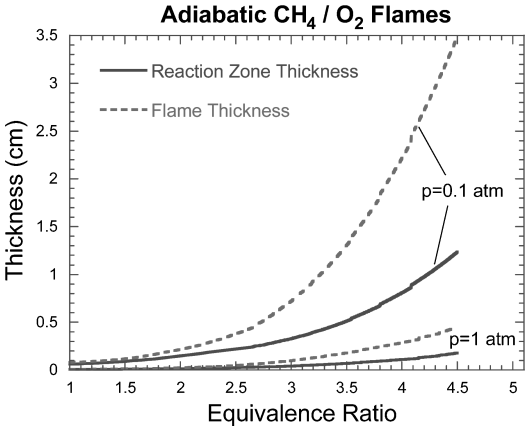

Fig. 1 Variations of flame thickness and reaction zone thickness of adiabatic rich CH_4/O_2 flames as function of ER at pressures of 0.1 and 1.0 atm.

The flame structures for adiabatic, freely propagating, planar CH_4/O_2 flames at varying equivalence ratios were calculated using the PREMIX computational program.[24] The detailed gas-phase chemistry, thermodynamic properties, and transport properties were taken from GRI-Mech 3.0 (Ref. 25), including 53 species and 325 reaction steps. Calculations were conducted with the initial temperature of 300 K and pressures ranging from 0.1 to 1.0 atm.

Figure 1 shows the characteristic flame dimensions, including flame thickness and reaction zone thickness, of adiabatic rich CH_4/O_2 flames as a function of equivalence ratio for 0.1 and 1.0 atm. The flame thickness is determined by calculating the difference between the final and initial temperatures and dividing by the maximum temperature gradient within the flame, whereas the reaction zone thickness is defined as the full width of one-half of the maximum heat release rate profile. As expected, both flame dimensions increase with increasing rich equivalence ratio. It is also seen that the flame dimensions increase with decreasing pressure. Specifically, the flame thickness at 1.0 atm and equivalence ratio (ER) = 4.5 is 0.5 cm, whereas that at 0.1 atm and ER = 3.5 is 1.3 cm. Moreover, the reaction zone thickness at 1.0 atm and ER = 4.5 is 0.2 cm, and that at 0.1 atm and ER = 3.5 is 0.55 cm. These results show that the flame thicknesses of the aforementioned rich mixtures are larger than the diameter of the 0.4- and 0.8-mm platinum tubes used in experiments, and, hence, the microtube diameters are smaller than the associated quenching diameter.

To determine the flammability limits for CH_4/O_2 flames, the PREMIX program was modified to include radiative heat loss and the capability to solve equations at singular points. The radiation heat loss in the optically thin limit due to CO, CO_2, H_2O, and CH_4 was included because these are considered to be the major radiative species in CH_4/O_2 flames. The Planck mean absorption coefficients are a function of temperature and were obtained from Refs. 26–28. As the program continues the calculation from the stable branch to the unstable branch, the program passes through the turning point creating numerical stiffness, especially with the detailed chemical kinetics. To solve this problem, the flame controlling continuation method[29] was utilized in this study. The analysis was performed to determine the rich flammability limits for CH_4/O_2 flames at different pressures. Figure 2a shows such radiative flame response curves by plotting mass burning flux vs ER. The corresponding flame response curves in terms of maximum temperature are shown in Fig. 2b. The turning point, beyond which steady flame propagation is not possible, defines the flammability limit. It is seen that the rich flammability limit decreases as pressure is decreased. The rich flammability limit occurs at ER = 4.5 for atmospheric pressure and at ER = 3.6 for a pressure of 0.1 atm. Furthermore, Fig. 2b indicates that the maximum temperatures are generally above 1450 K within the flammable regime. To prevent overheating the microtube, fuel-rich conditions between ER = 6 and 10 were tested to keep the maximum temperature at a reasonable level. As such, all of the test

conditions were beyond the fuel-rich flammability limits calculated in Fig. 2.

Experimental Setup

The experimental setup included a vacuum chamber with a test stand, microtube, mass flow control system, data acquisition system, power supply for heating the microtube, vacuum pump, and infrared (IR) camera. The vacuum chamber was outfitted with a test stand to hold the experimental setup. The test stand included ceramic insulators for mounting the microtube and a bulkhead to hold the flow connections. The chamber was also equipped with a feedthrough that included thermocouple leads and pressure transducer wiring as well as a ZnSe window for taking IR images and several observation windows.

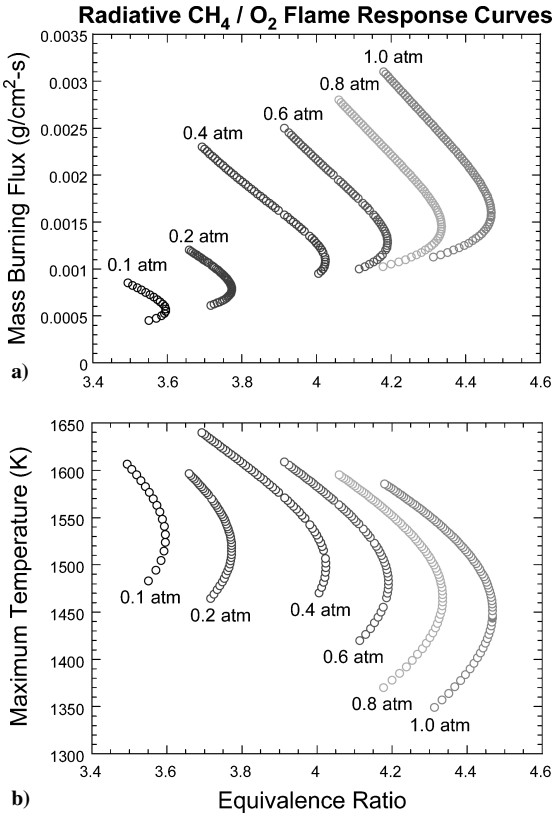

Fig. 2 Radiative flame response curves of CH_4/O_2 flames at varying pressures, in terms of a) mass burning flux and b) maximum temperature; stable (unstable) branch is upper (lower) portion of curve.

Microtubes were chosen because their simple geometry can be used for fundamental numerical simulations and they are easy to fabricate from readily available materials. The study utilized 0.4- and 0.8-mm inside diameter platinum tubes with overall lengths of 100 mm and 200 mm, respectively. The microtube included two nickel tabs soldered at 15 and 85% of the tube length so that 70% of the tube length was heated. The heating was achieved utilizing a dc power supply connected to the nickel tabs. The tube also had a stainless-steel extension tube soldered to the entrance to allow for connection with the flow system. Thermocouples (TC1, TC2, and TC3) were welded to the tube at 29, 50, and 71% of the entire tube length, respectively. At the exit of the tube, a fine-gauge R-type thermocouple, TC exit, was used to measure the exit temperature. These thermocouples were critical for this testing because they allowed the preheat temperature to be determined and also gave an indication of whether combustion was present in the tube.

The mass flow system included the Unit Instruments mass flow controllers for O_2, CH_4, and H_2. A sonic nozzle was also used to meter higher flow rates of O_2. Once the desired flow rates were set, the fuel and oxidizer flowed into a mixing chamber where they were directed into an exhaust hood until ready for experimental use. A three-way solenoid valve was used to switch the flow into the tube when starting the experiment.

The data acquisition system included a National Instruments SCXI-1000 chassis for acquiring signals from thermocouples, pressure transducers, and mass flow controllers, as well as for recording the voltage across the tube. The data acquisition system also included a relay module for switching the three-way solenoid valve as desired. A schematic of the test cell is shown in Fig. 3.

Computational Methodology

Microtube experiments were simulated using the PLUG code,[30] including detailed gas-phase and surface chemistry via CHEMKIN[31] and Surface CHEMKIN[32] interpreters. In the plug-flow model it is assumed that there is no mixing in the axial direction and perfect mixing in the transverse direction. The model also assumes that axial diffusion of any quantity is negligible relative to the convective term, which is particularly valid in high-speed flow conditions. Raja et al.[33] suggested practical bounds for which

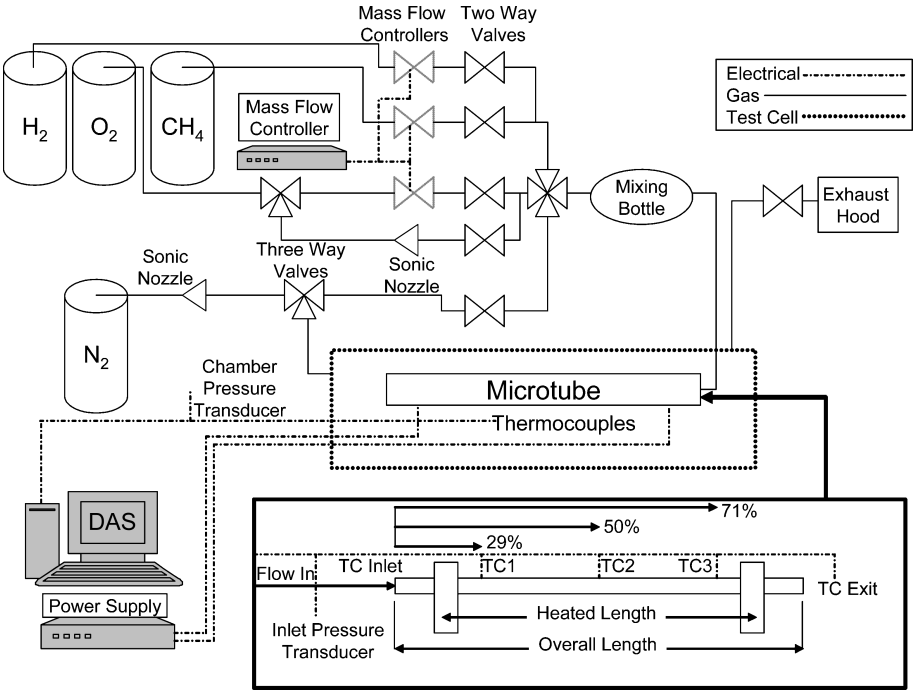

Fig. 3 Schematic of microtube test setup.

the plug-flow assumption is valid, namely, $D/L \ll Re_D Sc \ll L/D$, where D is the inside tube diameter, L the tube length, Re_D the Reynolds number based on tube diameter, and Sc the Schmidt number. Based on this criterion, the plug-flow model is valid for all of the cases tested. It is also noted that $Re_D Sc$ shows a decrease as pressure is decreased and when catalytic combustion occurs. Similar to the experimental setup, the computational configuration included a centrally located heated section of length L_h, for which a uniform heat flux Q was applied. In addition, the wall thickness was assumed to be infinitely thin, and heat loss through the tube wall to the surroundings was not considered herein.

Governing equations employed can be found in Ref. 30. The friction force exerted on the gas mixture by the microtube wall was considered in the momentum equation, and the friction factor is assumed to be a function of Re_D (Ref. 30). For laminar flow, the friction factor is $f = 16/Re_D$, whereas for turbulent flow the Blasius formula is utilized.[30] When calculating the mixture viscosity, the PLUG program was modified to include detailed evaluations of transport properties in conjunction with the TRANSPORT package.[34] The gas-phase kinetics mechanism employed was GRI-Mech 3.0 (Ref. 25), and the surface kinetics mechanism was taken from Deutschmann et al.,[35] including 11 surface species and 24 surface reaction steps. Although the aforementioned two widely used reaction mechanisms have not been extensively validated over the range of the present test conditions, their adequacy and validity in describing the associated fuel-rich ignition/combustion phenomena can be assessed through the comparison of experimental and computed results.

Experimental Results

The experimental results consisted of a determination of critical ignition temperature, an examination of self-sustainability, and an assessment of microtube performance parameters. In each case the heated section of the tube was exposed to a voltage, leading to resistive heating of the tube. The preheat temperature was read from TC2, which was shown to be the maximum recorded temperature in the tube before flowing the gaseous mixture. This is because heat loss to the electrical leads and ends of the tube caused the temperatures of TC1 and TC3 to be reduced from TC2. Because of material limits imposed by the soldered joints on the microtubes, the maximum preheat temperature tested was limited to be <1040 K. At each ER and flow rate, the preheat temperature was gradually increased until catalytic ignition occurred. An IR camera was used for qualitative analysis, but the spatial resolution was insufficient to warrant an accurate quantitative measurement of tube temperature distribution. Once ignition was achieved and steady state was maintained, the power supply was turned off to see if the catalytic reactions were capable of self-sustenance. It was shown that for self-sustaining reactions, the steady-state temperature reading is independent of preheat temperature, whereas it is dependent on equivalence ratio, mass flow rate, and ambient pressure.

General Experimental Trends

Indication of exothermic reactions was determined by monitoring the temperature data recorded and the tube inlet pressure. For an experiment that does not ignite, the temperatures will decrease to a steady-state value below the preheat temperature, as demonstrated in Fig. 4a. When combustion occurs, it is seen from Fig. 4b that the three thermocouples on the tube (TC1–TC3) show an increase in temperature above the designated preheat temperature, that is, at time $= 0$. In addition, the steady-state inlet pressure will exhibit a step increase when combustion occurs, as shown in Fig. 5, giving a separate indication of the ignition event.

Also note that during microtube testing two different modes of ignition were observed. The first mode was ignition initiating in the downstream portion of the tube. Ignition within this mode can be further classified into two distinctly different conditions: ignition after a time delay or instant ignition. The delayed ignition phenomenon was seen at low flow rates near the critical ignition temperature. After a certain time delay, some exothermic reactions released enough heat for catalytic ignition to take place. The delayed ignition usually

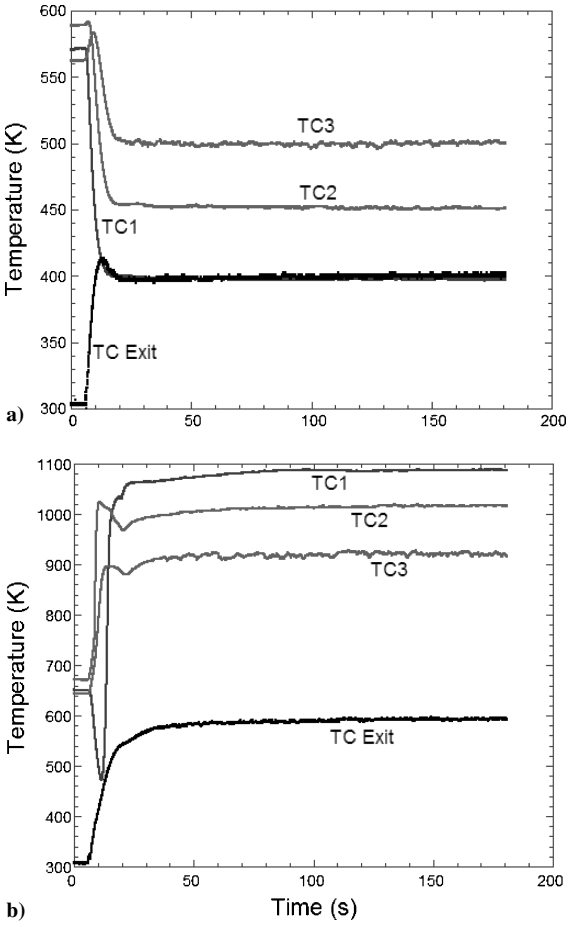

Fig. 4 Sample time variations of thermocouple readings data for an 0.8-mm Pt tube at ambient pressure of 1.0 atm: a) nonreacting case with imposed heat flux of 2.168 W/cm^2 and b) reacting case with imposed heat flux of 2.839 W/cm^2; mixture condition, ER of 8.0 and mass flow rate of 0.008 g/s.

initiated downstream and propagated upstream, with catalytic combustion taking more than 100 s to initiate. The second downstream ignition phenomenon occurred within 20 s of starting the mixture flow and was considered as instant ignition because of the relatively shorter ignition delay. This instant ignition phenomenon was common at all flow rates with intermediate preheat temperatures. The second mode of ignition was instant ignition in the upstream portion of the tube and was common for high preheating temperatures. These results suggest that preheat temperatures near the critical temperature should be avoided if rapid ignition is desired.

Figure 6 further demonstrates the time variations of temperatures and inlet pressure for a reacting case in which the power and, therefore, the imposed heat flux were turned off approximately 380 s after the mixture flowed in the microtube. Figure 6 shows that after the heat flux was stopped, whereas the temperatures and inlet pressure decreased to new steady-state values, the catalytic reactions were self-sustaining for the given conditions.

The effect of mass flow rate on the critical preheat temperature was examined using the current setup. Figure 7 shows a sample of the raw experimental data for an 0.8-mm Pt tube at an ambient pressure of 1.0 atm and ER $= 8$. When these data are used, the ignition limit or critical ignition temperature is determined based on the onset of ignition, as shown in Fig. 7. Note that the actual critical ignition temperature lies somewhere between the reacting and nonreacting case, but that it can be fairly sharply delineated by experiment. Once the steady-state reactions were able to be achieved, the combustion temperature, although dependent on the mass flow rate, applied heat flux, and exit ambient pressure, was found to always be above the critical ignition temperature, as demonstrated in Fig. 4b. Furthermore, note that for most of the vacuum conditions

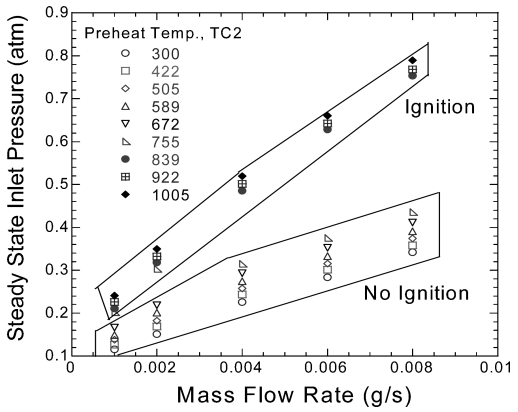

Fig. 5 Steady-state inlet pressures with different preheat temperatures and mass flow rates for 0.8 mm Pt tube at ambient pressure of 0.0136 atm; mixture ER is 8.0.

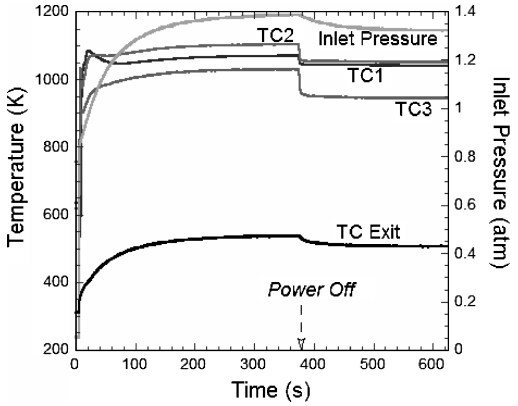

Fig. 6 Sample time variations of temperature and inlet pressure for 0.4-mm Pt tube at ambient pressure of 0.0136 atm, showing steady-state operation with and without applied heat flux; mixture condition: ER of 8.0 and mass flow rate of 0.004 g/s.

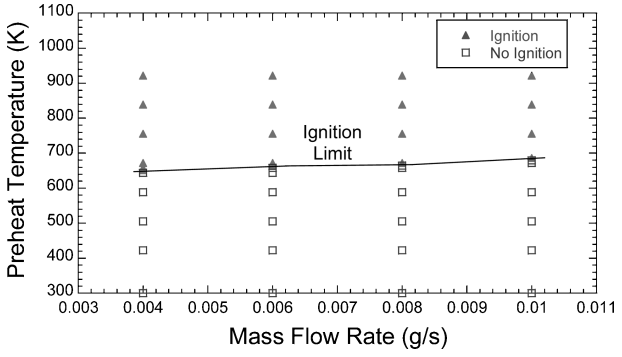

Fig. 7 Preheat temperature vs mass flow rate for 0.8-mm Pt tube with ER = 8 and ambient pressure of 1.0 atm, demonstrating determination of critical ignition temperature.

tested herein, the flow inside the microtube was choked frictionally. It was also observed that the addition of imposed heat flux and heat release via reactions help initiate choking in the tube. On the other hand, none of the tests with an ambient pressure of 1.0 atm were choked with the mass flow rates available. Understanding of the choking condition is important for the performance optimization of a microthruster. The following sections will discuss the observed trends in the ignition limits at varying conditions.

0.4-Millimeter Platinum Tube Results

Figure 8a shows critical temperature vs equivalence ratio for the 0.4-mm platinum tube. The 1.0-atm tests were carried out at mass flow rates of 0.002, 0.004, and 0.006 g/s. The global residence time, defined as the tube length divided by the inlet velocity, ranged from

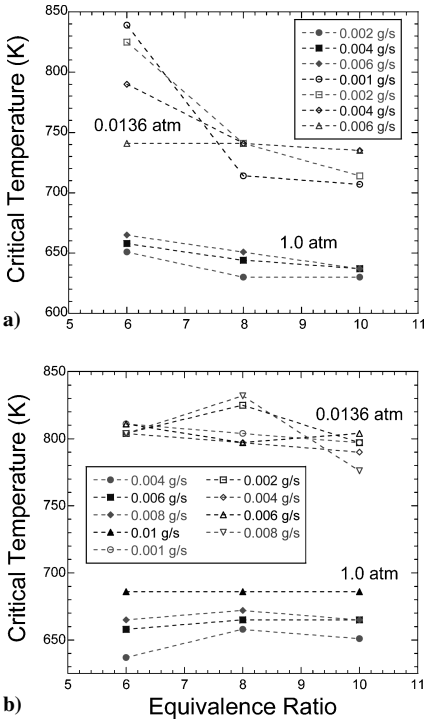

Fig. 8 Critical ignition temperature as function of ER at ambient pressures of 1.0 (filled symbols) and 0.0136 atm (open symbols): a) 0.4-mm Pt tube and b) 0.8-mm Pt tube.

3 to 6.5 m/s. Note from Fig. 8a that critical temperature increases with increasing mass flow rate and decreases with an increase in ER. At ER = 6, critical temperatures ranged from 651 to 665 K. At ER = 10, critical temperatures ranged from 630 to 637 K. The decreasing critical temperature with increasing ER was consistent with the study by Deutschmann et al.[35] For all 1.0-atm cases, the minimum nonreacting inlet pressure was 1.05 atm and the maximum reacting inlet pressure was 2.07 atm.

The vacuum tests (ambient pressure of 0.0136 atm) were conducted with flow rates of 0.001, 0.002, 0.004, and 0.006 g/s. The corresponding global residence times ranged from 2.5 to 6 m/s. Figure 8a shows that the critical temperatures were higher than those of the 1.0-atm tests for all flow rates and equivalence ratios investigated. The minimum critical temperature at ER = 6 was 740 K, and the maximum was 839 K. The minimum critical temperature at ER = 10 was 707 K and the maximum was 740 K. At the lowest mass flow rate, 0.001 g/s, the delayed ignition phenomenon was observed, but the delayed ignition temperature was not considered to be the critical temperature because the proposed thrusters will require fast ignition times. The inlet pressures were a minimum of 0.27 atm for nonreacting flow and a maximum of 1.95 atm for reacting flow.

Self-sustaining reactions were achieved at all flow rates and ER tested using 0.4-mm Pt tube. The peak tube temperature readings for ER = 6 and 10 can be as high as ∼1200 and ∼1000 K, respectively. In general, the steady-state temperature is increased with higher mass flow rates. Although the data showed a decrease in temperature moving downstream, the maximum value of TC3 ranged from ∼530 K to ∼1100 K.

0.8-Millimeter Platinum Tube Results

The 1.0-atm tests were conducted at mass flow rates 0.004, 0.006, 0.008, and 0.01 g/s, which covered the range of global residence time from 9 to 22 m/s. Figure 8b shows that the critical temperature increases as mass flow rate increases. Contrary to the 0.4-mm tube, the 0.8-mm tube does not show a trend as ER is changed. Namely, the critical temperature variation with ER was found to be small for a given flow rate. At ER = 6 the critical temperature was between 637 and 686 K, whereas at ER = 10, the critical temperature ranged from 651 to 686 K. The minimum inlet pressure was 1.02 atm for

nonreacting flow, and the maximum inlet pressure was 1.36 for reacting flow. Comparison of the calculated exit velocity, by assuming pressure matching and sonic velocity at the exit, indicated that none of the atmospheric tests were choked.

The vacuum tests (at 0.0136 atm) were conducted at mass flow rates 0.001, 0.002, 0.004, 0.006, and 0.008 g/s, corresponding to global residence times of 6–16 ms. Again, Fig. 8b shows that the critical temperatures for the 0.0136-atm tests were higher than those of the 1.0-atm tests. The minimum critical temperature at ER = 6 was 804 K, and the maximum critical temperature at ER = 6 was 811 K. At ER = 10 the minimum critical temperature was 776 K, and the maximum was 804 K. The delayed ignition phenomenon was noticed at flow rates of 0.001 g/s for all ER tested and 0.002 g/s for ER = 8 and 10. The minimum inlet pressure was 0.12 atm, and the maximum inlet pressure was 0.82 atm. For all reacting flow cases, the exit velocity was assumed to be sonic, because the computed exit velocity assuming pressure matching was higher than the exit sonic velocity for all cases.

Self-sustaining reactions were observed at all flow rates for the 1.0-atm cases using an 0.8-mm Pt tube. For the 0.0136-atm tests, self-sustaining reactions were observed for flow rates between 0.004 and 0.008 g/s. For low flow rates of 0.001 and 0.002 g/s blowout was observed. The blowout was most likely caused because the heat loss was greater than the heat release once the power was turned off. The data for all cases showed a decrease in steady-state temperature moving downstream, whereas the steady-state temperatures at each location were seen to be higher when the flow rate was increased. The range of steady-state temperatures achieved for the 0.8-mm Pt tube is similar to that for the 0.4-mm one.

0.4-Millimeter Platinum Tube Results with Hydrogen Doping

Because previous work showed that H_2/O_2 combustion in catalytic tubes exhibited much lower critical temperatures[10,20] than CH_4/O_2 as described earlier, the effect of adding hydrogen to CH_4/O_2 mixtures was studied. For all cases studied, a constant H_2 mass flow rate of 0.0001 g/s was added to the rich CH_4/O_2 mixture, which, therefore, raised the effective ER. For the ER = 6 and 10 tests with 0.001 g/s of CH_4/O_2, the effective ERs are increased to approximately 8 and 13, respectively. All of the flow rates and ERs reported in the following text are based on the CH_4/O_2 mixture only; however, the additional mass of hydrogen was included when evaluating the performance parameters. The CH_4/O_2 flow rates considered were the same as the 0.4-mm Pt tube without hydrogen addition.

Note in the hydrogen doping experiments that the ignition limit was somewhat sensitive to the preceding test run on the catalytic tube. To eliminate this memory effect, it was necessary to flow an inert gas through the tube for extended periods of time between runs. The ignition data obtained using this methodology are thought to be fairly accurate, but the repeatability of some of the trials at lower temperatures can be questioned. All of the reported critical temperatures correspond to the maximum critical temperatures observed. Figure 9 shows the critical temperature as a function of ER at different flow rates and ambient pressures.

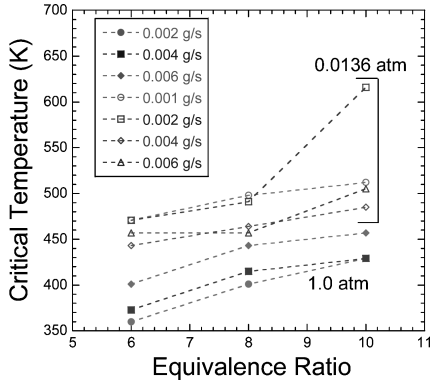

Fig. 9 Critical ignition temperature as a function of ER with H_2 doping (0.0001 g/s) at ambient pressures of 0.0136 (open symbols) and 1.0 atm (filled symbols), 0.4-mm Pt tube.

At 1.0 atm, the addition of hydrogen lowered the critical temperature significantly. For ER = 6 and a flow rate of 0.002 g/s the critical temperature was 360 K, and at 0.006 g/s it was 400 K. The inlet pressures ranged from 1.02 atm for nonreacting cases to 2.21 atm for 0.006 g/s with ignition. For ER = 10 the critical temperature increased from 429 K at 0.002 g/s to 457 K at 0.006 g/s. The inlet pressure ranged from 1.07 atm for 0.001 g/s without ignition to 2.11 atm for 0.006 g/s with ignition. As a comparison, the critical temperatures for rich H_2/O_2 mixtures reported by Boyarko et al.[10] and Boyarko[20] ranged between 350 and 375 K for global residence times of 2–7 ms. Hence, hydrogen addition aids ignition even for such fuel-rich conditions. Figure 9 also shows that the critical temperature increased as ER increased, which was opposite what was observed for CH_4/O_2 mixtures without H_2 doping. This could be because the amount of H_2 addition was fixed so that H_2 would dominate the ignition response at lower ERs due to a higher percentage of H_2 in the fuel mixture.

For vacuum tests, at ER = 6 ignition occurred between critical temperatures of 440 and 470 K for all flow rates investigated. At ER = 10 the range of ignition temperatures was then from 485 to 615 K. Although this ER = 10 case showed an overall increase in the critical temperature range from those observed in the 1.0-atm case, the critical temperature was reduced substantially as compared to the case without hydrogen addition. In addition, the inlet pressure for ER = 6 was 0.37 atm for a nonreacting case at 0.001 g/s and was 1.93 atm for a reacting case at 0.006 g/s. At ER = 10 the inlet pressure was 0.73 atm for a reacting case at 0.001 g/s and 1.73 atm for a reacting case at 0.006 g/s, both with a preheat temperature of 922 K. The delayed ignition phenomenon was observed for 0.001 g/s flow rates at ER = 8 and 10.

Self-sustaining reactions were observed at all flow rates for both the 1.0- and 0.0136-atm cases using a 0.4-mm Pt tube with H_2 doping. At 1.0 atm, the steady-state temperature decreased as the flow moved downstream. For the 0.0136-atm case the temperature decreased as the flow moved downstream for low flow rates, but faster flow rates had a maximum temperature in the middle of the tube. In general, the maximum steady-state temperature achievable was slightly reduced with hydrogen doping. This is simply because under such fuel-rich conditions the addition of H_2 lowers the final equilibrium temperature.

Microtube Performance

The goal of this investigation is ultimately to aid the development of a microthruster for space applications, capable of producing 1–10 mN of thrust. In the following text, the thrust and specific impulse are presented as a function of mass flow rate, and the required power to achieve this thrust level is subsequently discussed. The thrust calculations were conducted for the vacuum tests because they will be most applicable to space exploration. In each case, the exit velocity was assumed to be sonic, and the exit temperature was taken as the steady-state value of TC3 due to the much larger uncertainty in the exit thermocouple reading. Additionally, the mean molecular weight and specific heat ratio were estimated using a chemical equilibrium program.[36] Although the present calculated thrust values may appear optimistic, the associated uncertainty is expected to be within 20%.

0.4-Millimeter Platinum Performance

Figure 10a shows the thrust vs mass flow rate for the 0.4-mm Pt tube. At each flow rate, the ER = 6 cases had the highest thrust output. At 0.006 g/s, 11 mN of thrust could be generated with combustion, as opposed to 5.5 mN without catalytic ignition, showing that the catalytic combustion effectively doubled the output thrust. At a flow rate of 0.001 g/s, about 1.5 mN of thrust can be generated.

Figure 10b shows the performance assessment in terms of specific impulse. The specific impulse was highest for ER = 6. This is because the resulting steady-state temperature was slightly higher. The maximum specific impulse is 190 s at a flow rate of 0.006 g/s. Without ignition the maximum specific impulse was 100 s at 0.002 g/s, and so catalytic reactions effectively raised the specific impulse. Furthermore, the heating power required to achieve combustion in

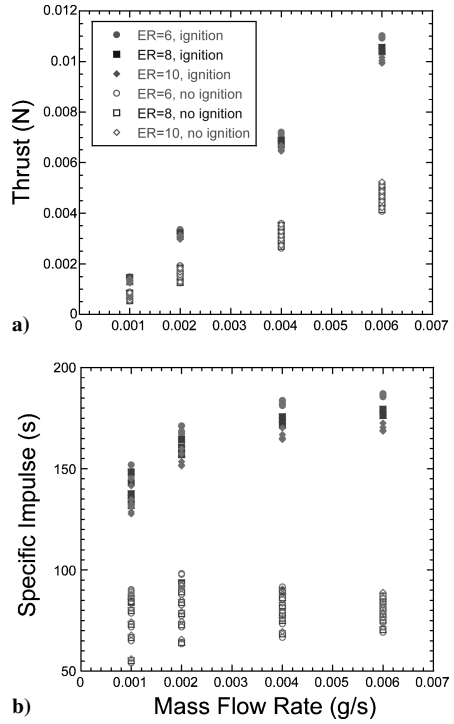

Fig. 10 Performance of 0.4-mm Pt tube at varying ER and mass flow rates: a) thrust and b) specific impulse; 0.0136 atm.

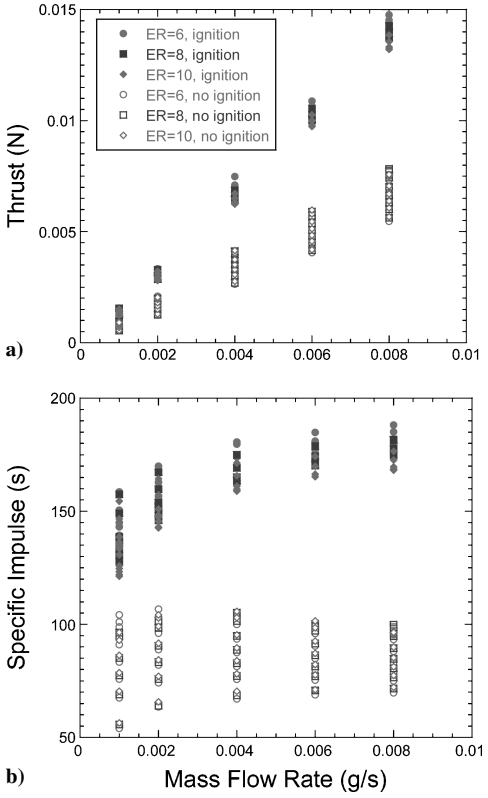

Fig. 11 Performance of 0.8-mm Pt tube at varying ERs and mass flow rates: a) thrust and b) specific impulse; 0.0136 atm.

most cases was about 3.5 W. Near maximum thrust of 11 mN could be obtained at power inputs of 3.6–5.8 W, showing the small effect of an increase in heating power on thrust output.

0.8-Millimeter Platinum Performance

Figure 11 shows the resulting thrust and specific impulse vs mass flow rate for the 0.8-mm Pt tube. As with the 0.4-mm platinum data, the ER = 6 case generated maximum thrust at all flow rates with a maximum of 14.8 mN at 0.008 g/s. The maximum thrust generated at a mass flow rate of 0.001 g/s with combustion was 1.5 mN. As a result, the expected thrust range was about 1.5–14.8 mN for the flow rates tested. Maximum thrust without catalytic ignition was 7.8 mN at 0.008 g/s, showing that catalytic reactions almost double the thrust output. In addition, the specific impulse was highest for ER = 6. The maximum specific impulse was 190 s for the 0.008-g/s case, which is the same as for the 0.4-mm tube. Specific impulses between 180 and 190 s can be achieved with mass flow rates of 0.004, 0.006, and 0.008 g/s. The maximum specific impulse without catalytic ignition was 106 s, showing again the usefulness of catalytic reactions.

For ER = 6 with a mass flow rate of 0.008 g/s, ignition occurred with a heating power input of just over 6 W that yielded an available thrust of 14 mN, whereas the maximum thrust of 14.8 mN required 13 W. The lowest power input required to achieve ignition was observed at ER = 10 and a flow rate of 0.001 g/s and was 3.8 W, which generated 1.2 mN of thrust. Further increasing the power input to 12.7 W only increased thrust minimally to 1.5 mN. The preceding results, therefore, demonstrate that the extra power applied added only minimally to the thrust generated.

0.4-Millimeter Platinum Performance with Hydrogen Doping

Thrusts and specific impulses generated at varying mass flow rates and ERs for the 0.4-mm tube with hydrogen addition are shown in Fig. 12. The thrust levels were slightly higher than those seen in the 0.4-mm platinum tube without hydrogen because there is more mass flow with the addition of hydrogen. The maximum thrust was 11.4 mN at 0.006 g/s and 2 mN at 0.001 g/s. The maximum thrust for nonreacting flow was 4.7 mN at 0.006 g/s, showing that the catalytic combustion of CH_4/O_2 with H_2 doping can yield more than double the maximum thrust.

Maximum specific impulse was generated at a flow rate of 0.006 g/s, but specific impulses above 180 s could be generated at all flow rates tested. This can be attributed to the lower mean molecular weight of the mixture at low flow rates because there was a higher percentage of hydrogen than at the faster flow rates. Note that the maximum specific impulse without catalytic ignition was

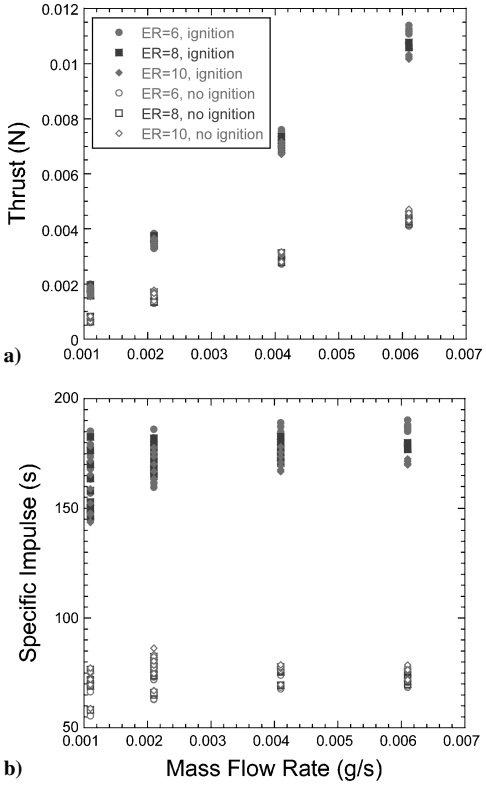

Fig. 12 Performance of 0.4-mm Pt tube with hydrogen doping (0.0001 g/s) at varying ERs and mass flow rates: a) thrust and b) specific impulse; 0.0136 atm.

85 s, which was lower than the case without hydrogen doping. The variation was caused by the difference in mean molecular weight and the higher exit temperatures of nonreacting CH_4/O_2 mixtures because their preheat temperature was higher.

Near maximum thrust was generated with as little as 1 W of power input as opposed to the 4 W required without the addition of hydrogen. When hydrogen doping is used, the power required to achieve ignition can be reduced by 75%, leading to a significant weight savings because a smaller power supply would be required to achieve ignition. Thus, further study that systematically investigates the effect of varying amounts of H_2 addition on the catalytic ignition/combustion of CH_4/O_2 mixtures is warranted.

Computational Results

Although a detailed transient simulation on microtube experiments including heat loss from the tube wall will be carried out in the future, the present steady-state plug-flow model for CH_4/O_2 mixtures was conducted to provide insight into the critical conditions leading to catalytic ignition, as well as the axial variations of gas temperature, flow velocity, gas pressure, gas-phase species composition, and site fraction of surface species. The inlet conditions were taken to be mixture temperature of 300 K, mixture velocity of 10 m/s, inlet pressure of 0.5 atm, and mixture composition of ER = 8. The viscosity was calculated using detailed transport properties at each numerical step. The geometry studied was that of the 0.4-mm platinum tube, and a uniform heat flux Q was applied to the center 70 mm of the tube, bounded by the dashed lines shown in Fig. 13.

Figure 13 shows the axial variation of temperature, pressure, and Mach number with different imposed heat fluxes. It is seen from Fig. 13 that catalytic ignition is achieved when Q is beyond 0.52 W/cm^2. As the heat flux is increased from 0.8 to 1.0 W/cm^2, the temperature rise and, therefore, the ignition location, occurs further upstream. The pressure drop across the tube tends to increase as the applied heat flux is increased. This pressure drop is due to the acceleration of the flow in the tube. As expected, the Mach number increases toward the tube exit with increasing applied heat flux. Figure 13b also indicates that as the heat flux is increased above 1.129 W/cm^2, the flow becomes choked somewhere in the tube, and steady-state solutions fail to exist for the given inlet conditions.

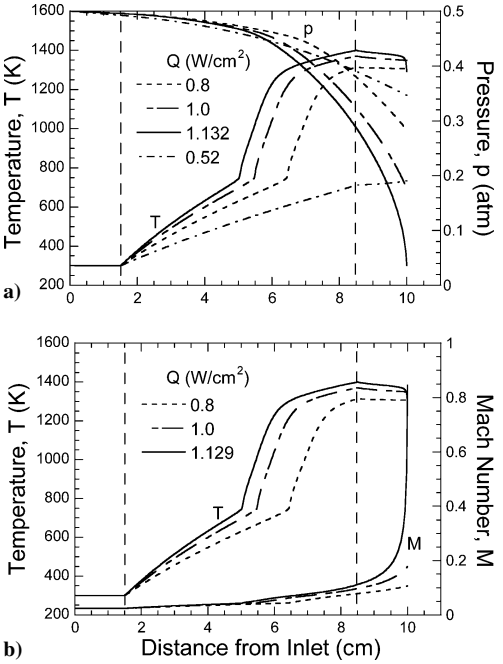

Fig. 13 Computed axial variations of a) temperature and pressure and b) temperature and Mach number, with varying applied heat fluxes; inlet temperature, pressure, and velocity are 300 K, 0.5 atm, and 10 m/s, respectively; ER = 8.0.

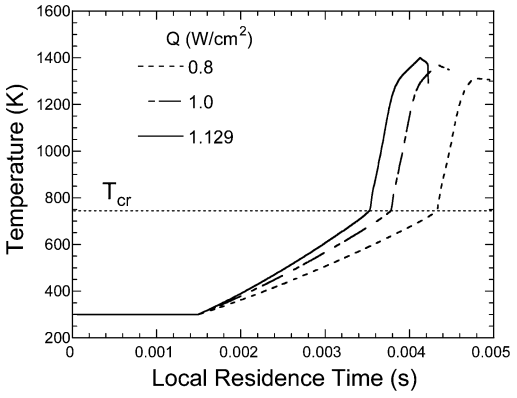

Fig. 14 Temperature variations vs local residence time with varying applied heat fluxes; inlet temperature, pressure, and velocity are 300 K, 0.5 atm, and 10 m/s, respectively; mixture ER = 8.0.

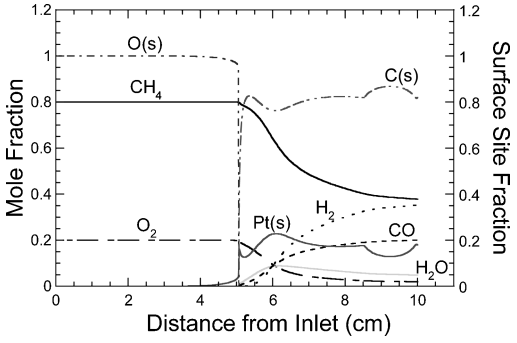

Fig. 15 Computed spatially resolved profiles of important gas-phase and surface species for 0.4-mm Pt tube with $Q = 1.129$ W/cm^2; inlet conditions: 300 K, 0.5 atm, 10 m/s, and ER = 8.

The resulting temperature profiles are plotted against local residence time in Fig. 14. Figure 14 shows that catalytic ignition is possible only when the local temperature exceeds a critical ignition temperature T_{cr}. This critical temperature occurring near 750 K is shown in Fig. 14 as a dotted line. This result is close to the experimental value obtained with ER = 8 at an ambient pressure of 0.0136 atm.

Figure 15 shows the spatial structure of the $Q = 1.129$ W/cm^2 case. In Fig. 15, the spatially resolved profiles of the mole fractions of gas-phase species and site fractions of surface species are shown as a function of downstream distance. The major gas-phase species considered are CH_4, CO, H_2, H_2O, and O_2, whereas the important surface species plotted are Pt(s), O(s), and C(s). For the present fuel-rich condition, H_2O is first formed, followed by increasing concentrations of H_2 and CO. Before combustion the surface is completely covered with O(s), and after sufficient preheat O(s) desorbs and bare Pt(s) surface sites become available to aid the reaction. The main surface species present after ignition are C(s) and Pt(s), with C(s) dominating around 80% of the surface sites.

Further study was conducted to compute the dependence of the critical ignition temperature on the ER and inlet pressure. Figure 16 shows that, for all inlet pressures computed, as the equivalence ratio is increased, the critical ignition temperature decreases, which is generally in agreement with the experimental data. The computed results also suggest that as the inlet pressure is reduced, the critical temperature decreases, which, however, does not agree with our experimental findings. This discrepancy could be attributed to two factors. First, the tube heat loss to the surroundings, which is expected to vary with the surrounding pressure, was not considered in the calculations. Second, the surface mechanism may need to be optimized at varying pressures. Further investigation in resolving such a discrepancy is warranted.

For the microtube conditions tested, the ERs were beyond the computed flammability limit. As such, it is expected that gas-phase

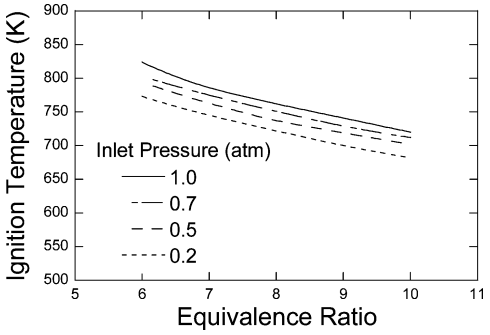

Fig. 16 Critical ignition temperature as function of ER at different inlet pressures; inlet temperature and velocity are 300 K and 10 m/s, respectively.

reactions account for only a small fraction of the observed heat release in the microtube experiments. To demonstrate the insignificance of gas-phase reactions, the results computed with and without gas-phase chemistry were compared. It was found that the two sets of computed results are essentially identical, indicating that, for the present modeling purposes, gas-phase reactions can be neglected.

Conclusions

Future microspacecraft will require new micropropulsion technology. The use of microchemical thrusters will, in turn, require the development of advanced microcombustors. The miniaturization of gaseous combustion systems, however, is restricted by the limitations on chamber dimensions. A viable alternative is to take advantage of surface combustion because catalytic reactions favor the increased surface area to volume ratio. The increased surface area as combustors are scaled down, combined with the favorable effects of surface catalysis, can be used to offset the quenching effects at small scales and further extend the fuel-rich flammability limit. Microtubes were chosen for this study because of their simple geometry and ease of fabrication. The microtube configuration can be easily implemented in fundamental simulations, allowing detailed characterization of the exit composition and temperature for validation purposes.

Platinum tubes with 0.4- and 0.8-mm inside diameters were tested at ambient pressures of 1.0 and 0.0136 atm. Detailed premixed CH_4/O_2 flame calculations showed that the ERs considered herein were beyond the gaseous fuel-rich flammability limit. Thermocouple data at three different locations along the tube, the temperature measured at the exit, and the inlet pressure were recorded as a function of time in resistively heated platinum tubes. These data were used to assess the progress of exothermic reactions along the catalytic tube. The test matrix included at least three flow rates at each ER and ambient pressure condition.

Significant surface reactions were found to take place in the 0.4- and 0.8-mm tubes at all conditions tested, provided that the imposed heat flux was high enough. Ignition location and characteristics, as well as steady-state temperature distribution, were found to depend on the imposed heat flux, mass flow rate, and ambient pressure. The use of small amounts of hydrogen was found to be helpful in reducing the critical ignition temperature and, thus, the power required to achieve ignition. It was also shown that, for most conditions tested, the catalytic reactions were able to self-sustain once ignited.

A plug-flow model with detailed gas-phase and surface chemistry was used to provide further insight into the present microtube experiments. Numerical results for CH_4/O_2 mixtures show that there is a characteristic critical temperature beyond which ignition occurs. This value was shown to depend only on the ER and inlet pressure. The computed critical temperature values agree reasonably well with the experimental data at the same conditions. Spatially resolved profiles of gas-phase mole fractions and surface site fractions show that the surface coverage is initially dominated by O(s). Once the critical temperature is reached, the surface subsequently becomes dominated by C(s) and Pt(s), leading to the consumption of CH_4 and O_2 and the formation of H_2, H_2O, and CO.

The required thrust of 1–10 mN can be obtained with flow rates in the range between 0.001 and 0.01 g/s. The specific impulse is typically between 180 and 190 s for reacting flow. The results show that, currently, a microthruster could be developed using as little as 1 W of power for ignition and that reactions could self-sustain if desired.

Acknowledgements

This work was supported by the NASA Microgravity Combustion Program with Merrill King as Contract Monitor. The first author would like to acknowledge fellowship support by the NASA Graduate Student Researchers Program.

References

[1]Micci, M., and Ketsdever, A. (eds.), *Micropropulsion for Small Spacecraft*, Progress in Astronautics and Aeronautics, AIAA, Reston, VA, 2000.

[2]Mueller, J., "Thruster Options for Microspacecraft: A Review and Evaluation of State-of-the-Art and Emerging Technology," *Micropropulsion for Small Spacecraft*, edited by M. Micci and A. Ketsdever, Progress in Astronautics and Aeronautics, AIAA, Reston, VA, 2000, pp. 45–137.

[3]Rossi, C., "Micropropulsion for Space—A Survey of MEMS-Based Microthrusters and Their Solid Propellant Technology," *Sensors Update*, Vol. 10, No. 1, 2002, pp. 257–292.

[4]Foster, J. E., "Compact Plasma Accelerator for Micro-Propulsion Applications," NASA [online database], URL: http://gltrs.grc.nasa.gov/reports/2001/TM-2001-211282.pdf [cited 6 July 2005].

[5]Phipps, C., Luke, J., Lippert, T., Hauer, M., and Wokaun, A., "Micropropulsion Using Laser Ablation," *Applied Physics A*, Vol. 79, Nos. 4–6, 2004, pp. 1385–1389.

[6]Oleson, S., Benson, S., Patterson, M., and Schreiber, J., "Radioisotope Electric Propulsion for New Frontiers Class Missions," *International Electric Propulsion Conference*, Paper IEPC-2003-0137, March 2003.

[7]Lewis, D., Jr., Janson, S., Cohen, R., and Antonsson, E., "Digital Micropropulsion," *Sensors and Actuators*, Vol. 80, No. 2, 2000, pp. 143–154.

[8]Tian, H., Zhang, T., Sun, X., Liang, D., and Lin, L., "Performance and Deactivation of Ir/γ-Al_2O_3 Catalyst in the Hydrogen Peroxide Monopropellant Thruster," *Applied Catalysis A: General*, Vol. 210, Nos. 1–2, 2001, pp. 55–62.

[9]Vieira, R., Bastos-Netto, D., Ledoux, M. J., and Pham-Huu, C., "Hydrazine Decomposition over Iridium Supported on Carbon Nanofibers Composite for Space Applications: Near Actual Flight Conditions Tests," *Applied Catalysis A: General*, Vol. 279, Nos. 1–2, 2005, pp. 35–40.

[10]Boyarko, G. A., Sung, C. J., and Schneider, S. J., "Catalyzed Combustion of Hydrogen–Oxygen in Platinum Tubes for Micro-Propulsion Applications," *Proceedings of the Combustion Institute*, Vol. 30, The Combustion Institute, Pittsburgh, PA, No. 2, 2005, pp. 2481–2488.

[11]London, A. P., Ayon, A. A., Epstein, A. H., Spearing, S. M., Harrison, T., Peles, Y., and Kerrebrock, J. L., "Microfabrication of a High Pressure Bipropellant Rocket Engine," *Sensors and Actuators A*, Vol. 92, Nos. 1–3, 2002, pp. 351–357.

[12]Baker, A. M., Curiel, A., Schaffner, J., and Sweeting, M., "You Can Get There From Here: Advanced Low Cost Propulsion Concepts for Small Satellites Beyond LEO," *Acta Astronautica*, Vol. 57, Nos. 2–8, 2005, pp. 288–301.

[13]Mungas, G., Das, D. K., and Kulkarni, D., "Design, Construction and Testing of a Low-Cost Hybrid Rocket Motor," *Aircraft Engineering and Aerospace Technology*, Vol. 75, No. 3, 2003, pp. 262–271.

[14]Yetter, R. A., Yang, V., Aksay, I. A., and Dryer, F. L., "Chemical Microthrusters: Combustion Issues and Approaches," *Chemical and Physical Processes in Combustion, The 2003 Technical Meeting of the Eastern States*, The Combustion Institute, Pittsburgh, PA, 2003, pp. III.1–III.5.

[15]Yetter, R. A., Yang, V., Aksay, I. A., and Dryer, F. L., "Combustion Issues and Approaches for Chemical Microthrusters," *Proceedings of the 6th International Symposium on Special Topics in Chemical Propulsion*, March 2005.

[16]Kappenstein, C., and Batonneau, Y., "Chemical Micropropulsion: State-of-the-Art and Catalyst Surface Requirements," AIAA Paper 2005-3920, July 2005.

[17]Fernandez-Pello, A. C., "Micropower Generation Using Combustion: Issues and Approaches," *Proceeding of the Combustion Institute*, Vol. 29, The Combustion Institute, Pittsburgh, PA, No. 1, 2002, pp. 883–899.

[18]Lloyd, S. A., and Weinberg, F. J., "A Burner for Mixtures of Very Low Heat Content," *Nature*, Vol. 251, Sept. 1974, pp. 47–49.

[19]Jeongmin, A., Eastwood, C., Sitzki, L., and Ronney, P. D., "Gas-Phase and Catalytic Combustion in Heat Recirculating Burners," *Proceedings of the Combustion Institute*, Vol. 30, The Combustion Institute, Pittsburgh, PA, No. 2, 2005, pp. 2463–2472.

[20]Boyarko, G. A., "Catalyzed Combustion of Hydrogen–Oxygen in Platinum and Palladium Tubes for Micropropullsion Applications," M.S. Thesis, Dept. of Mechanical and Aerospace Engineering, Case Western Reserve Univ., Cleveland, OH, May 2004.

[21]Williams, D. R., "A Crewed Mission to Mars," NASA [online article], URL:http://nssdc.gsfc.nasa.gov/planetary/mars/marssurf.html [cited 30 June 2005].

[22]Williams, F. A., *Combustion Theory*, 2nd ed., Addison Wesley Longman, Menlo Park, CA, 1985, pp. 268–284.

[23]Glassman, I., *Combustion*, 3rd ed., Academic Press, San Diego, CA, 1997, pp. 162–171.

[24]Kee, R. J., Grcar, J. F., Smooke, M. D., and Miller, J. A., "A FORTRAN Program for Modeling Steady Laminar One-Dimensional Premixed Flames," Sandia National Labs., Livermore, Rept. SAND85-8240, Dec. 1985.

[25]Smith, G. P., Golden, D. M., Frenklach, M., Moriarty, N. W., Eiteneer, B., Goldenberg, M., Bowman, C. T., Hanson, R. K., Song, S., Gardiner, W. C., Jr., Lissianski, V. V., and Qin, Z., "GRI-Mech 3.0," URL:http://www.me.berkeley.edu/gri_mech/ [cited 29 June 2005].

[26]Soufiani, J., and Taine, J., "High Temperature Gas Radiative Property Parameters of Statistical Narrow-Band Model for H_2O, CO_2 and CO, and Correlated-K Model for H_2O and CO_2," *International Journal of Heat and Mass Transfer*, Vol. 40, No. 4, 1997, pp. 987–991.

[27]T'ien, C. L., "Thermal Radiation Properties of Gases," *Advanced Heat Transfer*, edited by B. T. Chao, Univ. of Illinois Press, Urbana, IL, 1967, pp. 253–324.

[28]Hubbard, G. L., and T'ien, C. L., "Infrared Mean Absorption Coefficients of Luminous Flames and Smoke," *Journal of Heat Transfer*, Vol. 100, May 1978, pp. 235–239.

[29]Nishioka, M., Law, C. K., and Takeno, T., "A Flame-Controlling Continuation Method for Generating S-Curve Responses with Detailed Chemistry," *Combustion and Flame*, Vol. 104, No. 3, 1996, pp. 328–342.

[30]Larson, R. S., "PLUG: A FORTRAN Program for the Analysis of Plug Flow Reactors with Gas-Phase and Surface Chemistry," Sandia National Labs. Rept. SAND96-8211, Livermore, Jan. 1996.

[31]Kee, R. J., Rupley. F. M., and Miller, J. A., "Chemkin-III: A FORTRAN Chemical Kinetics Package for the Analysis of Gas-Phase Chemical and Plasma Kinetics," Sandia National Labs. Rept. SAND96-8216, Livermore, May 1996.

[32]Coltrin, M. E., Kee, R. J., Rupley, F. M., and Meeks, E., "Surface Chemkin-III: A FORTRAN Program for Analyzing Heterogeneous Chemical Kinetics at a Solid Surface–Gas Phase Interface," Sandia National Labs., Rept. SAND96-8217, May 1996.

[33]Raja, L. L., Kee, R. J., Deutschmann, O., Warnatz, J., and Schmidt, L. D., "A Critical Evaluation of Navier–Stokes, Boundary Layer, and Plug-Flow Models of the Flow and Chemistry in a Catalytic-Combustion Monolith," *Catalysis Today*, Vol. 59, No. 1-2, 2000, pp. 47–60.

[34]Kee, R. J., Dixon-Lewis, G., Warnatz, J., Coltrin, M. E., and Miller J. A., "A Fortran Computer Code Package for the Evaluation of Gas-Phase, Multicomponent Transport Properties," Sandia National Labs. Rept. SAND96-8246, Livermore, March 1998.

[35]Deutschmann, O., Schmidt, R., Behrendt, F., and Warnatz, J., "Numerical Modeling of Catalytic Ignition," *Proceedings of the Combustion Institute*, Vol. 26, The Combustion Institute, Pittsburgh, PA, No. 1, 1996, pp. 1747–1754.

[36]McBride, B. J., and Gordon, S., "Computer Program for Calculation of Complex Chemical Equilibrium Compositions and Applications," NASA, Reference Pub. 1311, June 1996.